https://doi.org/10.5194/egusphere-2025-4325
Preprint. Discussion started: 21 October 2025

Evaluation of evapotranspiration partitioning models in the Amazon forest

Long-Xiao Luo [1], Jun Lei [2], Zheng-Hong Tan [3,*]

[1] Institute of International Rivers and Eco-security, Yunnan University, Kunming 650504, China; luolongxiao@stu.ynu.edu.cn

[2] School of Ecology and Environment, Hainan University, Haikou 570228, China; Jun_Lei@foxmail.com

[3] School of Ecology and Environmental Science, Yunnan University, Kunming 650504, China; tan@ynu.edu.cn

* Correspondence: tan@ynu.edu.cn; Tel.: 86-138-7635-0711

Highlights

- The deviation of the ET simulation is smaller in savanna (RMSE=10.4 mm/month) than in the rainforest (RMSE=17.6 mm/month)
- Different models vary greatly for Ei and Es simulations
- The Ei part of models is too sensitive to temperature (17%) and radiation (12.5%)

Abstract

Although models that simulate actual ET have been widely used globally, their performance in tropical forests is unsatisfactory. The distribution of ET components is one of the key reasons. In this study, we evaluated the ability of three ET models (Forest-CEW, PML-V2, and PT-JPL) in a complex forest by analyzing their components. The data comes from seven ground-based eddy covariance flux towers in Brazil, which are part of the "Large Scale Biosphere-Atmosphere Experiment in Amazonia" (LBA) project. Our study found that the R^2 of Forest-CEW was 0.64, that of PT-JPL was 0.43, and that of PML-V2 was only 0.29. The average results of the model show that

https://doi.org/10.5194/egusphere-2025-4325
Preprint. Discussion started: 21 October 2025

T/ET=63.2%±16%, Ei/ET=32.3%±16%, and Es/ET=6%±5%. The model simulates better results in Savanna (RMSE=10.4 mm/month) than in the rainforest (RMSE=17.6 mm/month). Rn is the main driving variable of the model ET and T, with a sensitivity of 20%, temperature is the main driver of Ei, accounting for 17%, and LAI is the main driver of Es, but it produces a negative effect (-22.5%). Our analysis emphasizes the differences in the ability of existing models to simulate ET dynamics in complex forests. Improving the formulation of ET components, particularly the canopy interception part, holds significant potential for substantially enhancing the accuracy and reliability of these ET models.

Keywords: evapotranspiration, transpiration, canopy interception, canopy interception, ET model

1. Introduction

Forest hydrological cycles are a core component of the terrestrial hydrological cycle, playing a crucial role in regulating energy balance and biogeochemical cycles (Bonan, 2008; Fisher et al., 2017). Forest evapotranspiration (ET) primarily consists of three components: vegetation transpiration (T), canopy interception evaporation (Ei), and soil evaporation (Es). The proportion of Ei and Es varies depending on the ecosystem type. In forests with dense vegetation, the canopy's shielding effect on radiation transmission significantly influences these proportions. Due to the complex and highly covered canopy structure, solar radiation attenuates while penetrating the canopy, resulting in insufficient energy reaching the ground surface (Duarte et al., 2021; Matsuo et al., 2021), thereby limiting soil moisture evaporation. Conversely, canopy interception accounts for a larger proportion in forests (Gu et al., 2018). During rainfall events, part of the precipitation is captured on leaves, branches, and trunks, which is subsequently returned to the atmosphere through evaporation. This portion constitutes 15-30% of the total ET (Lopes et al., 2020; Singh and Szeicz, 1979). This high ratio of canopy interception is more pronounced in tropical forests due to their denser and multilayered canopy structures (Kalácska et al., 2005). Transpiration (T) establishes the mechanism for

https://doi.org/10.5194/egusphere-2025-4325
Preprint. Discussion started: 21 October 2025

water transfer from soil to atmosphere and is a key process for understanding plant water use efficiency and vegetation dynamics over time and space. It is considered a crucial link in the terrestrial water balance (Schlesinger and Jasechko, 2014). Additionally, T represents the largest water flux from land, but its quantification has a big uncertainty. Observational studies show that the global annual average T/ET is 0.61±0.15 (Schlesinger and Jasechko, 2014), but the results from some LSM models are high, at 0.70±0.09 (Fatichi and Pappas, 2017).

ET monitoring is now widely carried out around the world. The eddy covariance flux tower technique quantifies energy (latent heat flux, LE) and gas exchanges between ecosystems by measuring the covariance between vertical wind speed and scalar fluctuations (Shuttleworth et al., 1984). The widespread application of this technique has significantly advanced our understanding of the seasonal and interannual variability of tropical forest ET. Furthermore, understanding the driving mechanisms of ET processes by environmental factors such as rainfall, radiation, and temperature is important in the refined application of ET models (Costa et al., 2010; da Rocha et al., 2009; Fisher et al., 2009; Fisher et al., 2008; Gomis-Cebolla et al., 2019; Morillas et al., 2013).

The ET model based on remote sensing remains the primary method for estimating large-scale ET fluxes, by combining the data from the EC flux site, the model was calibrated to greatly improve the accuracy of large-scale simulation. However, even if the total ET estimates are consistent, there are still significant differences in the components of ET (Miralles et al., 2016). Although the Sap Flow Method can effectively observe transient T, the difficulties in equipment installation and calibration make it challenging to cover large areas (Gao et al., 2022; Maes et al., 2020). Canopy interception is a very well-established study (Carlyle-Moses and Gash, 2011, Cuartas et al., 2007), but these data are often scattered in different locations and are neither comprehensive nor complete. This hinders the calibration of ET components. Currently, it is difficult to evaluate the performance of ET model partitions using sufficient observational data, but we try to propose improvement methods by taking advantage of the differences between different models and the correspondence between models and physical processes.

https://doi.org/10.5194/egusphere-2025-4325
Preprint. Discussion started: 21 October 2025

We employed three process-based ET models (capable of independently separating transpiration and evaporation processes) across seven different types of Amazonian forests. These include four pristine tropical rainforests, two seasonal forests (one of which is flood-stressed), and one tropical savanna. Our goal is to provide the proportions and seasonality of different components of ET in the Amazon forest. In addition, we will analyze the mechanism and sensitivity of different models. We expect that these different ET models will provide a broad perspective for exploring the seasonality of ET and its components.

2. Materials

2.1. The study site and meteorological data

The study site was in South America, and we used original flux data from the Large-Scale Biosphere Atmosphere Experiment in Amazonia (LBA) eddy covariance towers in the Brazil flux network. The LBA integrated data collected on nine observation towers in the Amazon of Brazil, including eddy covariance fluxes for carbon and energy, meteorological parameters, radiation, canopy temperature, humidity and CO_2 profiles, and soil moisture and temperature profiles (Restrepo-Coupe et al., 2013).

We selected data from 7 sites (Figure 1), including Manaus (K34), Santarém tropical moist forest towers (K67 and K83), and Caxiuana (CAX) close to the city of Belém (Pará) in northeastern Brazil (Carswell et al., 2002), which were typical of tropical rainforests in the Amazon basin; Reserva Jarú (RJA) was a seasonal forest located in the southern Amazon (Kruijt et al., 2004); although remote sensing data showed that Pe de Gigante (PDG) was a tropical woodland savanna site, in reality it was mainly composed of closed shrubs and small trees (5 m tall), sparse tall trees (7-10 m tall), dense herbaceous, and to a lesser extent almost closed trees up to 10 m tall (Batalha, 1997; Rocha et al., 2002), and research indicates that the LAI in this region can reach 6 m^2/m^2 (Restrepo-Coupe et al., 2013); Rio Javaes-Bananal Island (BAN) was a seasonally flooded ecotone about 2 km east of the Javaezinho river, which was

https://doi.org/10.5194/egusphere-2025-4325
Preprint. Discussion started: 21 October 2025

consisted of semi-deciduous forests, high woodland savannahs with a canopy height of 18 m, and sparse shrubs (Borma et al., 2009).

Table 1

Site Information Table

Site name (Shorthand)	Lat/Lon	Canopy height (m)	Tower height (m)	Biome type	Reference
Manaus (K34)	2.61S/60.21W	30–35	50	Tropical rainforest	(Gomis-Cebolla et al., 2019; Restrepo-Coupe et al., 2013)
Santarem (K67)	2.85S/54.97W	35–40	63	Tropical rainforest	(Restrepo-Coupe et al., 2013)
Santarem (K83)	3.01S/54.58W	35–40	64	Selectively logged tropical rainforest	(Gomis-Cebolla et al., 2019; Restrepo-Coupe et al., 2013)
Caxiuana (CAX)	1.72S/51.53W	30–35	51.5	Tropical rainforest	(Gomis-Cebolla et al., 2019; Restrepo-Coupe et al., 2013), (Carswell et al., 2002)
Reserva Jaru (RJA)	10.08S/61.93 W	30	60	Tropical wet and dry forest	(Gomis-Cebolla et al., 2019; Restrepo-Coupe et al., 2013)
Rio Javaes-Bananal Island (BAN)	9.82S/50.13W	18	42	Seasonally flooded, forest-savanna ecotone	(Borma et al., 2009)
Pe de Gigante (PDG)	21.62S/47.63 W	1–10	21	Savanna	(Rocha et al., 2002)

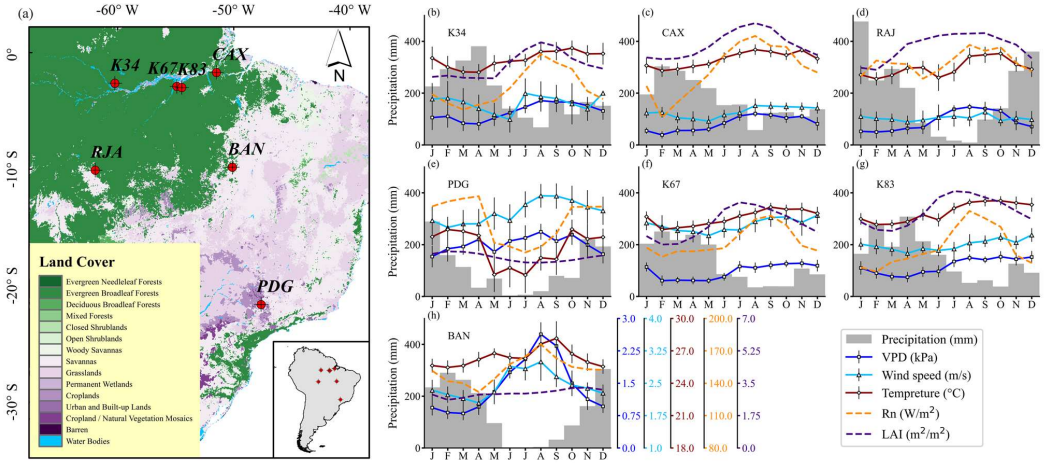

Fig. 1. Land cover of South America **(a)** along with the seasonal variations of precipitation, vapor pressure deficit (VPD), wind speed, temperature, net radiation

https://doi.org/10.5194/egusphere-2025-4325
Preprint. Discussion started: 21 October 2025

(Rn), and leaf area index (LAI) at each site **(b-h)**. The color of the lines in **(b-h)** corresponds to the color of the Y-axis values, and black vertical lines on the plot lines represent standard deviations. All Y-axes have the same scale.

There are many definitions of seasonality in tropical forests, and here we define the onset of the dry season as two consecutive months of precipitation of less than 100 mm (Luo et al., 2024). Environmental variables at the K34, CAX, K67, and K83 sites near the Amazon basin exhibited similar seasonal characteristics. Notably, all environmental variables showed an increasing trend at the onset of the dry season and began to decline midway or towards the end of the dry season. Although the K67 and K83 sites were relatively close to each other, the wind speed at the K67 site was higher.

The RJA site experienced abundant rainfall but also underwent a drier dry season with significant seasonal variation in precipitation. After entering the dry season, precipitation decreased by 64% and continued to decline to nearly no rainfall. During this period, environmental variables increased and then decreased after the dry season ended. Notably, the LAI at the RJA site was similar to that of the other four tropical rainforest sites.

Remote sensing data indicated that the PDG site had a lower LAI and exhibited significant environmental fluctuations (with high standard deviations), showcasing pronounced seasonality. Upon entering the dry season, wind speed and VPD at the PDG site increased but started declining midway through the dry season. Unlike other sites, at the PDG site, temperature and net radiation (Rn) rapidly decreased during the dry season and rebounded midway, with LAI showing a similar but less variable trend. Despite reduced rainfall from March to May, temperature and Rn continued to decline.

The BAN site featured a prolonged dry season. Precipitation decreased by 58% upon entering the dry season, followed by almost no rainfall for three subsequent months, gradually increasing afterward. During this period, VPD and wind speed displayed significant seasonal variation: they increased at the beginning of the dry season and weakened as precipitation recovered. Surprisingly, LAI at the BAN site showed almost no seasonal variation

https://doi.org/10.5194/egusphere-2025-4325
Preprint. Discussion started: 21 October 2025

throughout the dry season, and Rn showed a weak initial increase followed by a decline. Additionally, the BAN site experienced flooding from January to May each year, which might have impacted its ET (Fleischmann et al., 2023).

2.2. Vegetation data

The PML-V2 and PT-JPL models were originally designed for remote sensing, it requires two vegetation parameters, LAI and NDVI. LAI is using the Level-4 MODIS global Leaf Area Index (LAI) and Fraction of Photosynthetically Active Radiation (FPAR) product (MOD15A2H). This variable describe the dynamics of surface vegetation, and understanding how much rain will be intercepted by the vegetation canopy rather than falling to the ground. Normalized Difference Vegetation Index (NDVI) data is the Oak Ridge National Laboratory (ORNL) Distributed Active Archive Center (DAAC)'s product called "Global Vegetation Greenness (NDVI) from AVHRR GIMMS-3G+, 1981-2022" (Pinzon et al., 2023). NDVI is a spatial resolution of 0.0833 degree and global coverage from 1982 to 2022. NDVI is mainly used as an input to the PT-JPL model as a biophysical ability index to calculate the functional green leaf area fraction (Fisher et al., 2008).

3. Methods

We used three ET models: Forest-CEW, PML-V2, and PT-JPL, which can independently separate the two processes of transpiration and evaporation. Some of the models have been well applied and are considered to represent the expected average geographical patterns and seasonality (Melo et al., 2021; Miralles et al., 2016). Forest-CEW is a forest ecosystem process model we are currently developing. It simulates ecosystem vegetation dynamics by characterizing environmental biophysical and physiological processes. The aerodynamic part dealing with turbulent transport of matter and energy mainly references Campbell and Norman (Campbell and Norman, 1977), while aspects of radiation and energy balance are similar to the land-surface-transfer scheme (LSX) model (Pollard and Thompson, 1995). ET in Forest-CEW primarily consists of two parts: canopy interception and T, where canopy interception of

https://doi.org/10.5194/egusphere-2025-4325
Preprint. Discussion started: 21 October 2025

precipitation is expressed as a function of rainfall and leaf area index (LAI).

The PML-V2 and PT-JPL models are improvements based on the Penman-Monteith (PM) and Priestley-Taylor (PT) models (Penman and Keen, 1948; Priestley and Taylor, 1972). The PM model derives from the energy balance equation and not only includes solar and longwave radiation but also integrates factors such as temperature, humidity, and wind speed. As a simplified version of the PM model, PT is primarily driven by Rn since its aerodynamic component has been parameterized. Leuning and Fisher developed the Penman-Monteith-Leuning (PML) model and the Priestley-Taylor Jet Propulsion Lab (PT-JPL) model by integrating vegetation dynamics and meteorological factors into the models (Fisher et al., 2008; Zhang et al., 2010).

3.1. Forest-CEW model

Compared with the LSX model, Forest-CEW multiplies LAI by PAI to obtain the effective LAI and introduces a structural correction factor to adjust the interception coefficient. Evapotranspiration of Forest-CEW can be estimated by:

$$ET = T + \mathrm{E_i} \tag{1}$$

Transpiration (mm/hour) is assumed to occur only on the leaf surface, and the rate can be estimated by:

$$T = f_{str}(1 - f_{wet})2LAI\rho\frac{g_v g_s(q_s - q_p)}{g_v + g_s} \tag{2}$$

Where LAI is the leaf area index (m^2/m^2) and ρ is the air density (kg/m^3); g_v is the vapor conductance of leaf or stem surface (m/s); g_s is the stomatal conductance of gas ($mol/m^2/s$); f_{str} is the water stress factor, which can be calculated by (Santos and Costa, 2004):

$$f_{str} = \frac{1 - exp(-c_{str}AWI)}{1 - exp(-c_{str})} \tag{3}$$

Where c_{str} is the water stress coefficient; here c_{str}=-5. AWI is the available water indicator and can be described as:

$$AWI = \sum_{i=1}^{n}\frac{exp(-c_r \cdot i)}{-exp(-c_r \cdot i)/c_r} \tag{4}$$

https://doi.org/10.5194/egusphere-2025-4325
Preprint. Discussion started: 21 October 2025

Where n is the number of layers in which precipitation penetrates the soil; here n=4. c_r is the root profile factor; here c_r=1.5.

The fraction of wet surface is the ratio of water content on the surface to the maximum amount of water that the surface can withhold:

$$f_{\mathrm{wet}} = \mathrm{W_{wet}}/\mathrm{W_{max}} \tag{5}$$

Assuming δ_w is the thickness of water film on the surface (m), here $\delta_w = 0.001$, and ρ_w is the water density (kg/m^3), then:

$$W_{max} = 2LAI\delta_w\rho_w \tag{6}$$

During a rainy period, the surface of an object intercepts water E_i (mm/hour) and the water content on wet surface W_{wet} (kg/m^2) can be expressed as equations:

$$\mathrm{E_i} = f_{prec}[1 - exp(0.5LAI \cdot PAI)]Prec \tag{7}$$

Where f_{prec} is the structural factor for rain water interception; PAI is the plant area index (m^2/m^2); Prec is the precipitation (mm).

3.2. PML-V2 model

In PML-V2, ET is divided into transpiration (T), soil evaporation (E_s) and canopy intercepted evaporation (E_i). The formula used are as follows:

$$\lambda ET = \lambda T + \lambda E_s + \lambda E_i \tag{8}$$

$$\lambda \mathrm{T} = \frac{sA_c + \rho c_p}{\gamma} \mathrm{VPD} \cdot G_a \cdot \mathrm{s} + 1 + G_a/G_c \tag{9}$$

$$\lambda E_s = \frac{f \cdot s \cdot A_s}{s+1} \tag{10}$$

$$\lambda E_i = \begin{cases} f_v P & , P < P_{wet} \\ f_v P_{wet} + f_{ER}(P - P_{wet}), & P \geq P_{wet} \end{cases} \tag{11}$$

In the part of λT, where λ is the volumetric latent heat of vaporization (MJ/kg); s=Δ/γ, Δ is the slope of the saturation vapor pressure-temperature curve (kPa/C); γ is the psychrometric constant (kPa/C); ρ and c_p respectively

https://doi.org/10.5194/egusphere-2025-4325
Preprint. Discussion started: 21 October 2025

denote the air density for a given air pressure (kg/m^3) and the specific heat of air (MJ/kg/C); VPD is the vapor pressure deficit (kPa); A_c and A_s are respectively the net radiation for canopy and for soil (MJ/m^2/d), A_s=$R_n$exp(-0.61LAI) and A_c=Rn-A_s, in which LAI and R_n respectively represent the leaf area index (m^2/m^2) and the net radiation (MJ/m^2/d); G_a and G_c respectively represent the aerodynamic conductance (m/s) and canopy conductance (m/s), and were calculated using the formula:

$$G_a = \frac{k^2 u_m}{ln[(z_m-d)/z_{om}]ln[(zm-d)/z_{ov}]} \tag{12}$$

$$G_c = m\frac{P_1}{\kappa(P_2+P_4)}\left(\kappa LAI + ln\frac{P_2+P_3+P_4}{P_2+P_3\exp(\kappa LAI)+P_4}\right)\frac{1}{1+VPD/D_a} \tag{13}$$

Where k=0.41 represents von Karman's constant; z_m is the height at which wind speed and humidity are measured (m); u_m is the wind speed (m/s) at this height; d is the zero-plane displacement height (m); z_{om} and z_{ov} refer to the roughness lengths for momentum and the water vapor transfer, defined as z_{om}=0.123h and z_{ov}=0.1z_{om}, where h is the canopy height (m). In calculating G_c, m is the stomatal conductance coefficient; κ is the extinction coefficient for PAR; D_a is the water vapor pressure deficit of the air (kPa) (Gan and Liu, 2020). P_1, P_2, P_3, and P_4 are calculated as follows:

$$P_1 = A_m\beta I_0\eta, P_2 = A_m\beta I_0, P_3 = A_m\eta C_a, P_4 = \beta I_0\eta C_a \tag{14}$$

Where $A_m = 0.5V_m$; $V_m = \frac{V_{m,25}\exp[a(T_a-25)]}{1+\exp[b(T_a-41)]}$; in V_m, $V_{m,25}$ is the maximum catalytic capacity of Rubisco per unit leaf area at 25 °C (μmol/m^2/s); T_a is the air temperature (˚C); a=0.031 and b=0.115 are temperature coefficients (Li et al., 2023; Zhang et al., 2019). β [μmol/CO_2/(μmol/PAR)] and α [μmol/m^2/s/(μmol/m^2/s)] are initial slopes of the light and CO_2 response curve to assimilation rate, respectively. I_0 represents photosynthetically active radiation (PAR) (μmol/m^2/s); C_a represents CO_2 concentration (μmol/mol).

In the part of λE_s, f is the soil evaporation fraction that varies from 0 to 1. It is a function of the accumulated precipitation and soil equilibrium evaporation over a 32-day time step (Morillas et al., 2013; Zhang et al., 2010) and is calculated by:

https://doi.org/10.5194/egusphere-2025-4325
Preprint. Discussion started: 21 October 2025

$$f = \min\left(\frac{\sum_{n=1}^{N} P}{\sum_{n=1}^{N} E_{eqs}}, 1\right) \tag{15}$$

Where $E_{eqs} = \frac{sA_s}{(1+s)}$ represents the average equilibrium evaporation rate (mm/d) at the soil surface (Li et al., 2023); N=32 is the time step.

In the part of λE_i, f_v is the fractional area covered by intercepting leaves and f_{ER} is the ratio of average evaporation rate over average precipitation intensity storms; P and P_{wet} are respectively the daily precipitation (mm/d) and reference precipitation threshold of wet canopy (mm/d). f_v, f_{ER} and P_{wet} are the same as c, $\overline{E_c}$ and P'_G in the Gash model, which will be given later.

3.3. PT-JPL model

The equations are as follows:

$$\lambda ET = \lambda T + \lambda E_s + \lambda E_i \tag{16}$$

$$\lambda T = (1 - f_{wet}) f_g f_t f_m \alpha \frac{\Delta}{\Delta+\gamma} R_{nc} \tag{17}$$

$$\lambda E_s = [f_{wet} + f_{sm}(1 - f_{wet})] \alpha \frac{\Delta}{\Delta+\gamma} (R_{ns} - G) \tag{18}$$

$$\lambda E_i = f_{wet} \alpha \frac{\Delta}{\Delta+\gamma} R_{nc} \tag{19}$$

Where R_{nc} and R_{ns} are the same as A_c and A_s in PML-V2; f_{wet} is relative surface wetness, $f_{wet}=RH^4$ and RH is relative humidity. f_g is green canopy fraction, $f_g = \frac{f_{APAR}}{f_{IPAR}}$; where f_{APAR} and f_{IPAR} are the fraction of PAR absorbed by green vegetation cover and the fraction of PAR intercepted by total vegetation cover, $f_{APAR}=m_1SAVI+b_1$ (Gao et al., 2000) and $f_{IPAR}=m_2NDVI+b_2$ (Fisher et al., 2008); NDVI and SAVI are the normalized difference vegetation index and the soil adjusted vegetation index, SAVI=0.45·NDVI+0.132 (Gomis-Cebolla et al., 2019).

$$f_t = \exp\left[-\left(\frac{T_{max} - T_{opt}}{T_{opt}}\right)^2\right] \tag{20}$$

Where f_t is the green canopy fraction; T_{max} and T_{opt} are the maximum and optimum temperatures for plant growth (℃)

$$f_m = \frac{f_{APAR}}{f_{IPARmax}}, f_{sm} = RH^{VPD} \tag{21}$$

https://doi.org/10.5194/egusphere-2025-4325
Preprint. Discussion started: 21 October 2025

Where f_m and f_{sm} represent the water supply constraints for plant transpiration and the soil evaporation, respectively; VPD is the same as in PML-V2.

3.4. Model calibration

The model calibration was performed using the Bayesian optimization method. Bayesian optimization is a probabilistic model-based approach that efficiently finds the optimal solution in complex, high-dimensional, and computationally expensive parameter spaces. We constructed a Gaussian process as a surrogate model to guide the next step of the search, thus minimizing the number of trials required to find the optimal solution. When the specified accuracy and iteration count are reached, the algorithm outputs the optimal parameter combination and the value of the objective function. The calibrated model parameters are shown in Table 2. The parameters involved in the model are summarized in the supplementary materials.

Table 2

The optimized parameters of the models.

Model	Parameter	Unit	Value
Forest-CEW	f_{prec}	-	0.53
	g_s	$mol/m^2/s$	9.7
PML-V2	κ	-	0.5
	β	$\mu mol/CO_2/(\mu mol/PAR)$	0.09
	η	$\mu mol/m^2/s/(\mu mol/m^2/s)$	0.09
	$V_{m,25}$	$\mu mol/m^2/s$	15.8
	m	-	16.5
PT-JPL	T_{opt}	°C	24.3
	m_1	-	0.59
	m_2	-	0.2

https://doi.org/10.5194/egusphere-2025-4325
Preprint. Discussion started: 21 October 2025

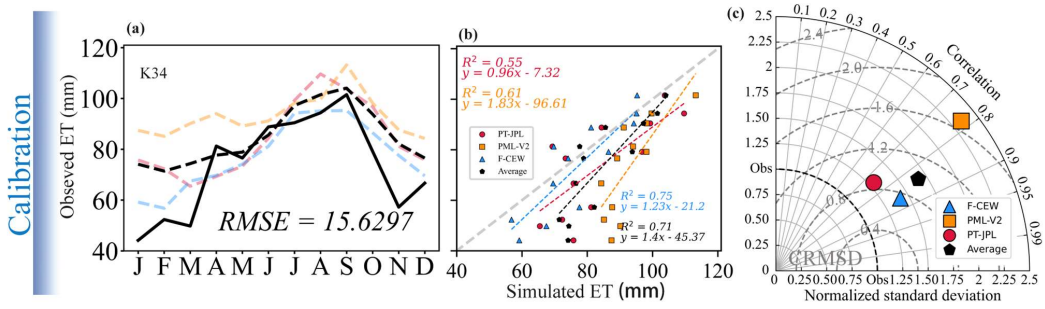

Fig. 2. (a) shows the model calibration result. The yellow dashed line represents the PML-V2 model, the red line represents the PT-JPL model, the blue line represents the Forest-CEW model, the black dashed line indicates the average results of the three models, and the black solid line represents the observed values; **(b)** shows the linear regression results of the observed and simulated values; **(c)** displays the statistical performance of the model as represented by a Taylor diagram.

This study used data from the K34 site for model calibration and the remaining six sites for model validation, and the optimization objective of the ET model is to minimize the root mean square error (RMSE) between the simulated ET and observed ET. Figure 2 presents the results of model calibration, showing small differences among the results simulated by the three models, but all models underestimated the ET values, particularly in the periods of higher precipitation. Importantly, the models were able to capture the seasonality of ET well, with the model averages showing a coefficient of determination of up to 0.71 compared to the measured ET.

4. Results

4.1 Models performance

https://doi.org/10.5194/egusphere-2025-4325
Preprint. Discussion started: 21 October 2025

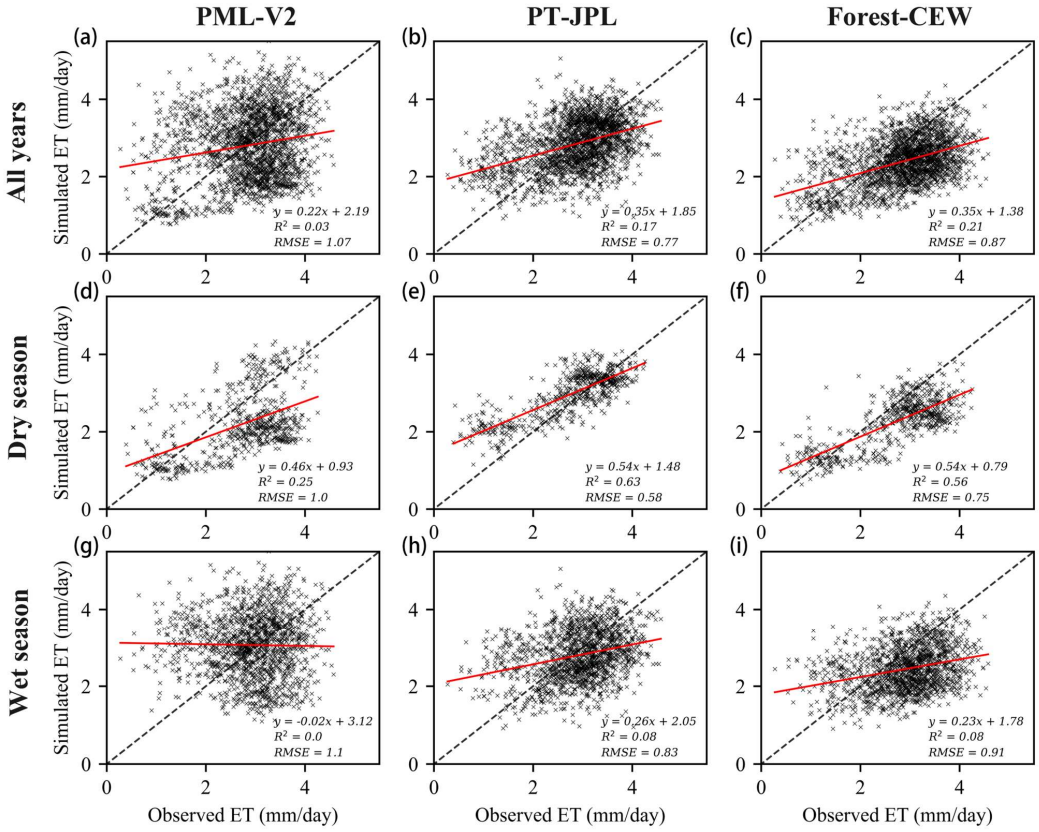

Fig. 3. The simulation results of different models throughout the year, during the dry season **(d-f)** and wet season **(g-h)**. The black dashed line represents the 1:1 line, and the red solid line represents the linear regression result.

The simulated time scale of the three ET models is daily, and subsequent analyses are aggregated to a monthly scale. Figure 3 shows the daily results of the different models simulating ET and comparing them to the observed ET. Obviously, the performance of the three models is comparable overall, but the PML-V2 appears to have a larger error than the other two. The simulation is easier in the dry season than in the wet season.

https://doi.org/10.5194/egusphere-2025-4325
Preprint. Discussion started: 21 October 2025

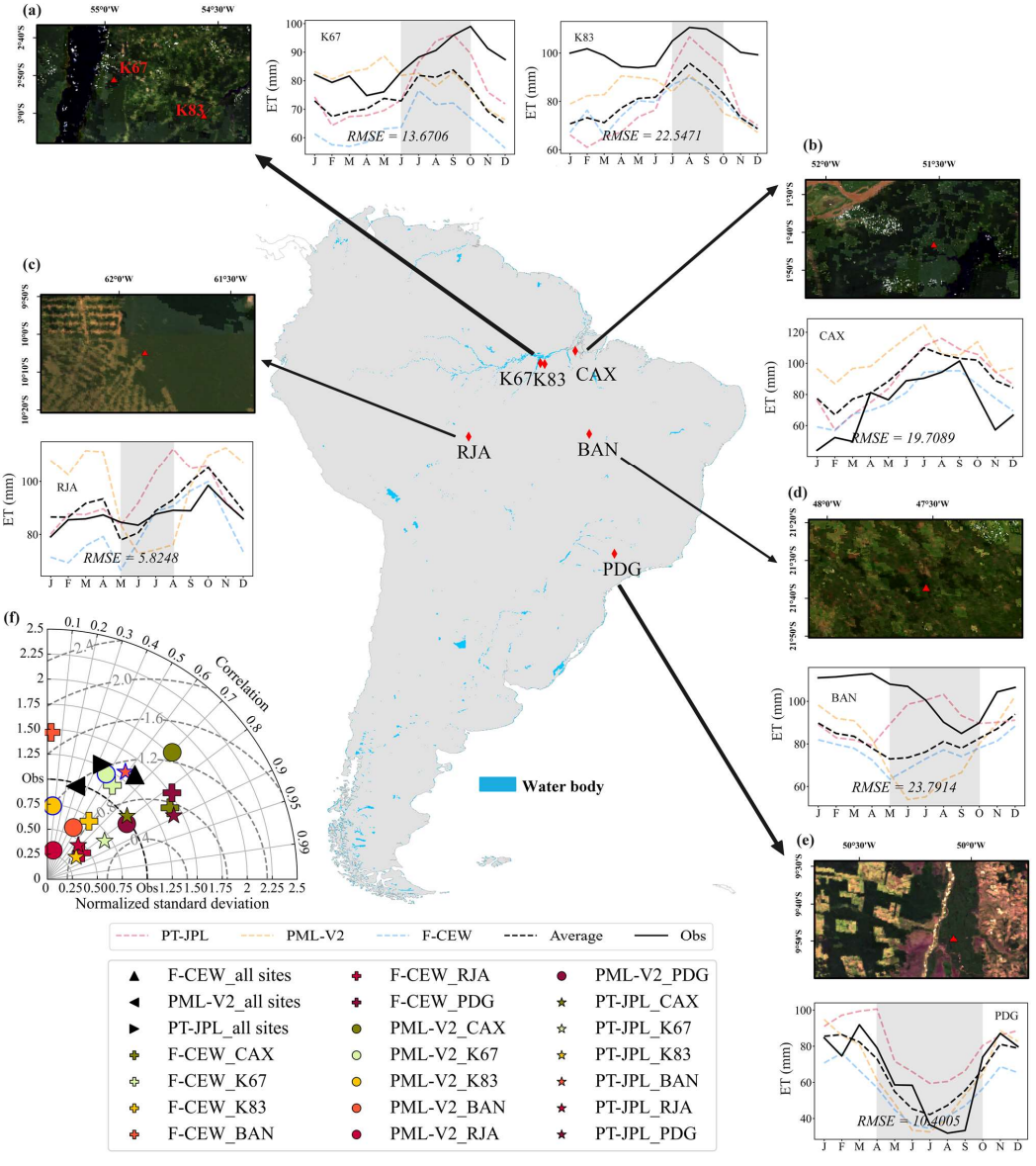

Fig. 4. (a-e) shows the true color RGB images (from NASA Land Processes Distributed Active Archive Center) and simulation results of each station. Gray shaded areas indicate dry seasons, solid black lines represent observed ET values, and dashed black lines denote model averages; **(f)** provides a statistical summary of the models' seasonality against observed values. Blue-edged markers denote negative correlations, while black-edged markers indicate positive correlations. Black-filled triangles represent aggregated data from all sites, with different triangle orientations indicating different models.

https://doi.org/10.5194/egusphere-2025-4325
Preprint. Discussion started: 21 October 2025

To better display the geographical features around the study area, we used satellite images from MODIS/Terra Surface Reflectance 8-Day L3 Global 500m SIN Grid V061; however, because the data is relatively old, the resolution is only 500 km. From the average results of the model, the simulation deviation values for the K67, K83, and BAN sites are large, especially for the BAN site, with an RMSE as 23.7914 mm/month. Besides the BAN site shows that the model average can capture the seasonality of ET well, and PT-JPL shows good results in K67 and K83, with correlation coefficients of 0.83 and 0.79 with the observed values. However, PML-V2 showed a negative correlation with the observed values at the K67 and K83 sites, and PT-JPL at the BAN site. We summarized the simulation results for all sites to observe the overall performance of the models (Figure 4 f black triangle markings), and found that the deviations from the observed values were relatively close for the three models, with an RMSE of 20.1674 mm/month for Forest-CEW, 22.4564 mm/month for PML-V2, and 17.8966 mm/month for PT-JPL. However, in terms of consistency with the observed values, Forest-CEW outperformed the other two models, with a correlation coefficient of 0.64, while PML-V2 only reached 0.29, and PT-JPL was 0.43.

We observed that the tropical rainforest sites near the Amazon river (CAX, K67, and K83) exhibited similar seasonality (Figure 4 a-e). Generally, ET displayed a unimodal trend, increasing initially and then decreasing. During the dry season, ET increased at the K67 and K83 sites. Although CAX did not experience a monitored dry season, the site received less precipitation from June to October, and ET also showed a similar increasing trend. At the RJA site, ET remained stable throughout the year without significant seasonal variation between the dry and wet seasons. PDG, located in an area with limited rainfall and a seven-month dry season, experienced almost no precipitation during its driest months. Observational data showed that ET at the PDG site exhibited significant seasonal variability, sharply declining by 65% at the start of the dry season and markedly rebounding in mid-dry season, closely matching the seasonal precipitation patterns. While BAN's ET seasonality was similar to PDG's, displaying a decrease-then-increase trend during the dry season, the magnitude of change was smaller. Additionally, the seasonal changes in

https://doi.org/10.5194/egusphere-2025-4325
Preprint. Discussion started: 21 October 2025

environmental drivers at BAN were opposite to those at PDG.

4.2 Proportionality, seasonality and variability of ET components

Figure 5 shows the annual totals of canopy interception, transpiration, and soil evaporation at each site, with three bar charts at each site representing the results of the Forest-CEW, PML-V2, and PT-JPL models. Overall, the simulation results of Forest-CEW were lower than those of PT-JPL and PML-V2. We found that at the BAN and PDG sites with lower vegetation coverage (average LAI of 3.3 m^2/m^2), only the PT-JPL model showed an increased proportion of soil evaporation. By comparing dry and wet season data, we observed that the proportion of T showed little difference between the dry and wet seasons. However, due to reduced precipitation, the proportion of Ei decreased during the dry season.

https://doi.org/10.5194/egusphere-2025-4325
Preprint. Discussion started: 21 October 2025

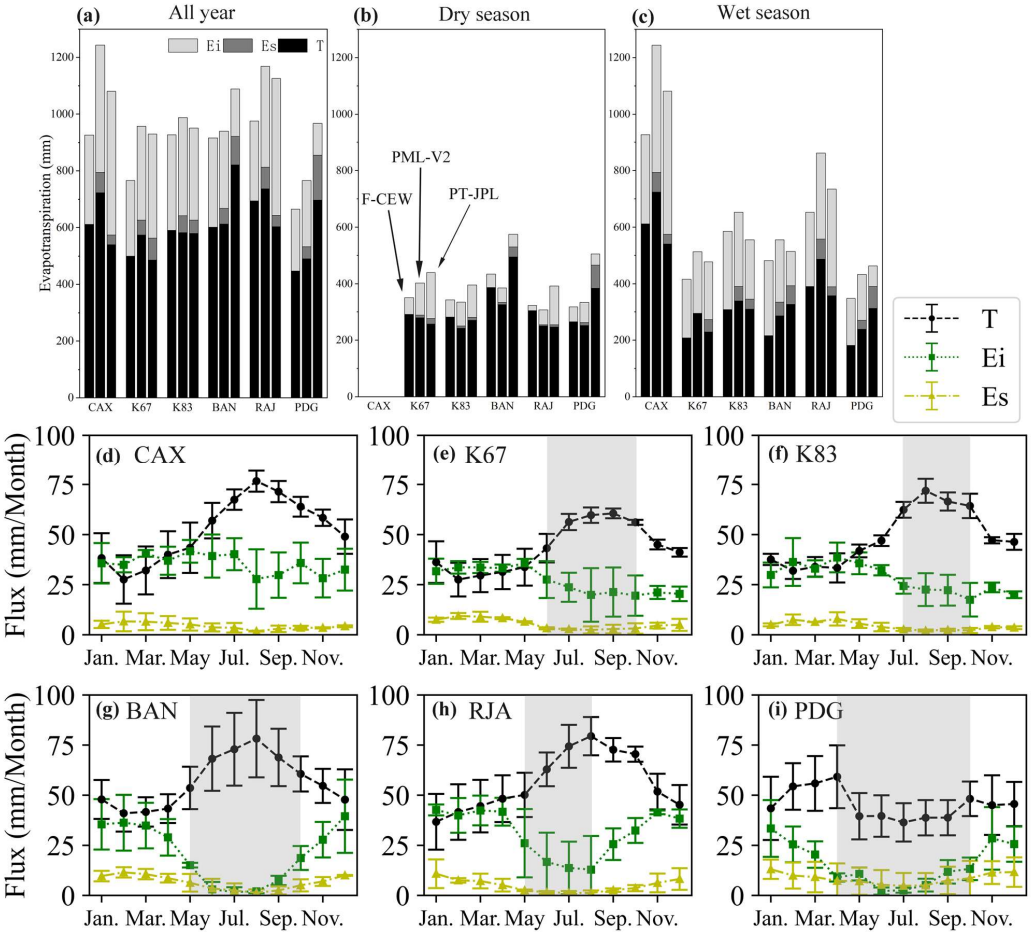

Fig. 5. (a-c) describe the ET components simulated by different models at each site, with three bar graphs per site representing Forest-CEW, PML-V2, and PT-JPL models, respectively. Light-colored bars represent canopy interception evaporation, medium-colored bars represent soil evaporation, and dark-colored bars represent vegetation transpiration. **(d-i)** shows the seasonal variations of transpiration, canopy interception, and soil evaporation, with the gray shading indicating the dry season and the error bars representing standard deviations.

We presented the trends in T, Ei, and Es, and it is clear that except for the PDG station, the T at other stations exhibits consistent seasonality, increasing at the beginning of the dry season and then decreasing in the middle or at the end. In contrast, Ei shows the opposite seasonality, starting to decline at the onset of the dry season, and exhibits a large standard deviation at the CAX, K67, and RJA stations, indicating that different models simulate the Ei process

https://doi.org/10.5194/egusphere-2025-4325
Preprint. Discussion started: 21 October 2025

differently. Overall, Es shows a seasonal variation of first increasing and then decreasing, and it is noteworthy that the large standard deviation at the PDG station indicates that the simulation results of the PML-V2 and PT-JPL models differ.

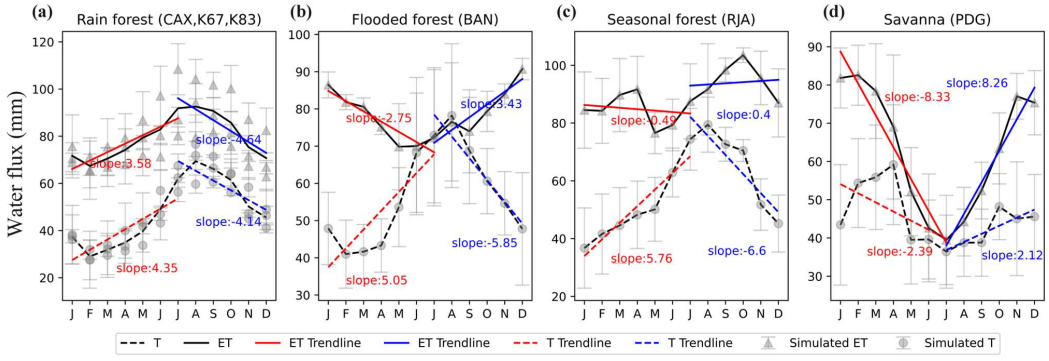

Fig. 6. (a-d) depict the variability of ET and T across different forest types. Gray triangle markers represent site-specific ET, gray circles represent site-specific T, and gray vertical lines indicate model standard deviations. Solid black lines denote average ET, and dashed black lines denote average T. Red solid lines represent the trend in the variation of ET during the first half-year, red dashed lines depict the trend in the variation of T during the first half-year, blue solid lines represent the trend in the variation of ET during the second half-year, and blue dashed lines represent the trend in the variation of T during the second half-year.

Figure 6 compares the variability of T and ET. The gray triangle represents the simulated ET of the site, and the error bar indicates the standard deviation of the three models. In addition, we consider the first half and the second half of the year separately based on the trends of ET and T, provide a trend line through linear regression, and use the slope of the linear regression as a quantification of the consistency between ET and T. The results show that only in tropical rainforests do T and ET both exhibit an increase-then-decrease trend, with the slope difference between the two not exceeding 1.5. At the BAN site, T and ET changed in completely opposite patterns, T slightly decreased early in the month, then sharply increased until August before plunging again, while ET gradually declined from early in the month until June, then rapidly decreased until September before surging again. At the RJA site, T showed a strong unimodal trend, peaking in August, while ET fluctuated minimally except for a slight increase in October. At the

https://doi.org/10.5194/egusphere-2025-4325
Preprint. Discussion started: 21 October 2025

PDG site, although T and ET followed the same trend, the amplitude of T change was much smaller than that of ET. From September to November, ET surged, while T only showed a slight increase. In addition, this figure reveals the differences between different models, and the standard deviation error bar shows that the variability in BAN, RJA and PDG is much greater than in rainforests.

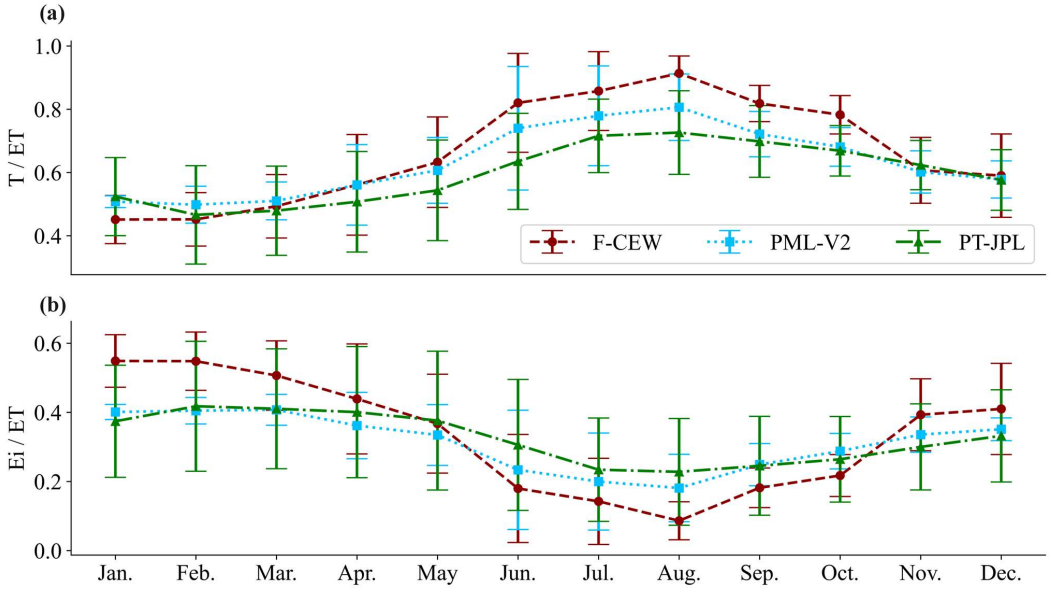

Fig. 7. (a) and **(b)** respectively show the proportions of T and Ei in ET along with their changing trends; different colors represent different models, and vertical lines indicate the standard deviation of different sites.

Figure 7 averages the sites, showing the changes in the three models T and Ei. During the wet season, the canopy intercepts more rain, but cloud cover leads to a decrease in net radiation (Rn), and the water film covering the leaf surface after the rain hinders transpiration. In the dry season, when precipitation decreases, the water intercepted by the canopy decreases or even disappears, while Rn and VPD increase, resulting in an increase in transpiration.

https://doi.org/10.5194/egusphere-2025-4325
Preprint. Discussion started: 21 October 2025

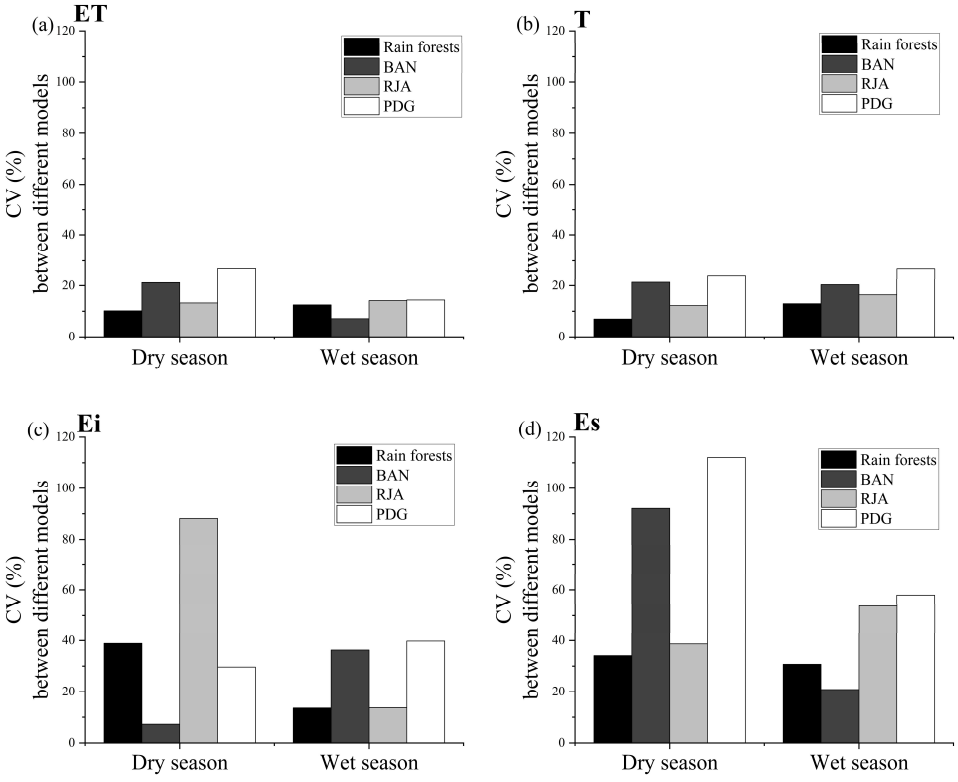

Fig. 8. (a-d) shows the variability of the simulation of ET and its components between different models, where rain forests are the average results of CAX, K67 and K83. Forest-CEW did not design Es, so **(d)** shows the result of PML-V2 and PT-JPL.

We quantified the simulation differences for ET and its components between different models by Coefficients of Variation (CV) at Figure 8. Obviously, the difference between Ei (33.4%) and Es (55%) is much greater than that between ET (14.9%) and T (17.6%). In addition, the simulation difference of the model for the dry season Ei at the RJA site is much greater than that in the wet season, and the same is true for the dry season Es at the BAN and PDG stations. Although Es accounts for only 10% of total ET, this part of the contribution will increase in forests with low LAI.

https://doi.org/10.5194/egusphere-2025-4325
Preprint. Discussion started: 21 October 2025

5. Discussion

5.1 Relationship between the unique characteristics of the sites and the ET

The various sites in the Amazon rainforest have unique characteristics due to differences in their geographical locations, vegetation types, and climatic conditions. Here, we attempt to analyze the characteristics of ET and its components in conjunction with the unique environments of each site. Manaus is located in the heart of the Amazon River and is primarily covered by tropical rainforests, boasting rich biodiversity. The climate is typically humid tropical, and ET can remain high due to abundant precipitation. K67 and K83 are also located near the Amazon River, significantly influenced by the Atlantic Ocean, with distinct wet and dry seasons and substantial annual precipitation. Although both sites are situated in tropical humid forests near Santarém, there may be slight differences in local vegetation types and canopy structures. As shown in Figure 1, K83 has a higher LAI, indicating it may have denser or taller trees, allowing for greater water interception and enhanced transpiration on the leaf surface.

Caxiuana is primarily characterized by lowland tropical rainforests with a complex multi-layered canopy structure. The higher LAI and increased precipitation at the CAX site result in relatively smooth seasonal variations of Ei. Overall, during the early dry season, precipitation decreases for CAX, K67, and K83, Rn increases, and the higher evaporation demand raises ET, enhancing Rn's control over ET. Reserva Jarú is mainly composed of evergreen broadleaf forests with high tree density and good vegetation cover. Despite the short dry season in RJA, precipitation drops to almost none after entering the dry season, yet the forest does not experience drought stress, as the abundant rainfall during the wet season allows the vegetation roots to extract water from deep soil (da Rocha et al., 2004).

The vegetation in PDG is characterized by sparse grasses and shrubs, which results in a generally low LAI. This lower LAI means that there is a reduced effective leaf surface area available for transpiration. The savanna's predominantly shallow root systems, coupled with significantly decreased rainfall during the dry season, limit the

https://doi.org/10.5194/egusphere-2025-4325
Preprint. Discussion started: 21 October 2025

plants' ability to access deep soil water. As surface soil water depletes, plants struggle to maintain high levels of transpiration, leading to a decrease in transpiration rates. Unlike dense broadleaf forests with their lush canopies, savanna plants may close their stomata due to intense radiation during the dry season, further inhibiting transpiration as a mechanism to conserve internal water. Moreover, the sparseness of the vegetation allows more radiation to penetrate through the canopy to the ground surface. Combined with higher temperatures, stronger wind speeds, and lower air humidity typical of the dry season, these conditions accelerate evaporation from the soil surface, indicating an increased proportion of soil evaporation within the total ET.

The BAN site is a seasonally flooded forest-savanna ecotone, but it exhibits very different environmental variables from PDG. During the extended and arid dry season at BAN, precipitation drops sharply and Rn increases as clouds diminish. Despite the increase in other environmental variables, ET begins to weaken. This pattern is a clear response characteristic of tropical savanna ecosystems, associated with the dry season's increased radiation and temperature. It occurs because this period typically features higher cloud cover and cooler temperatures, common in the transition zone between the Amazon rainforest and the Brazilian Cerrado climate regions (da Rocha et al., 2009b). It is worth noting that during the model evaluation phase (Fig. 4. d), the model did not capture the seasonality of ET well at the BAN site, which increased the risk associated with the results at the BAN site. Seasonal flooding could be one such factor (Fleischmann et al., 2023), but a more detailed explanation requires further investigation.

5.2 Improving the Ei module is important for ET partitioning

https://doi.org/10.5194/egusphere-2025-4325
Preprint. Discussion started: 21 October 2025

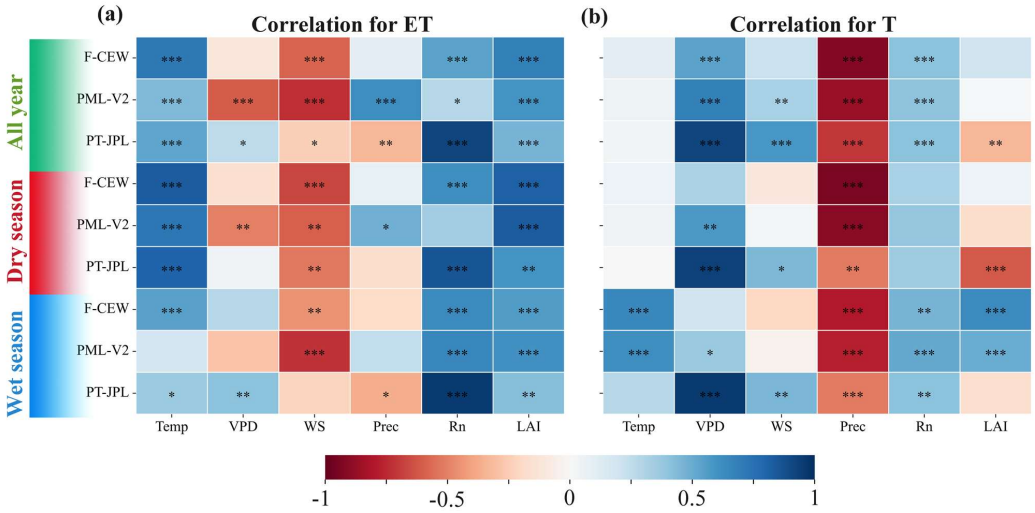

Fig. 9. (a, b) shows the influence of environmental variables on ET and T, evaluating variables including temperature (Temp), vapor pressure deficit (VPD), wind speed (WS), precipitation (Prec), net radiation (Rn), and leaf area index (LAI). The table colors indicate Pearson correlation values, with left-hand side colors representing sampling periods (all seasons, dry season, and wet season); * indicates significant correlation at P<0.05; ** at P<0.01; *** at P<0.001.

We analyze the environmental drivers of ET and T's seasonality through a simple relevance. Figure 9 shows the three factors most consistently correlated with ET across all three models: temperature, net radiation (Rn), and leaf area index (LAI). There is a close relationship between temperature and Rn; higher Rn typically leads to an increase in surface and near-surface air temperatures because more energy is absorbed and converted into heat. Additionally, higher VPD indicates drier air, which increases the intensity of plant T and exacerbates water loss (Grossiord et al., 2020).

By separating dry and wet season data, we found that Rn and temperature are key factors controlling the seasonality of ET. Many studies support this conclusion, especially in humid regions (Costa et al., 2010; da Rocha et al., 2009; Fisher et al., 2009; Restrepo-Coupe et al., 2021). What is more, a comprehensive study indicated that LAI and growth stages collectively account for 43% of the variation in global T/ET data sets (Wei et al., 2017). However, environmental factors such as Rn, VPD and water are also significant drivers (Ghimire et al., 2022; Kühnhammer et

https://doi.org/10.5194/egusphere-2025-4325
Preprint. Discussion started: 21 October 2025

al., 2023; Pieruschka et al., 2010). We do not fully understand the water stress impact from groundwater storage (Zhao et al., 2022), the dynamics of this part are unknown to us, but we have a very good understanding of the dynamics of environmental variables, and atmospheric demand has a significant impact on vegetation function (Novick et al., 2016).

VPD becomes the primary driver of T, and it is significantly negatively correlated with precipitation (Figure 9). In the absence of water stress, stomatal conductance regulates water vapor diffusion by controlling stomatal opening and closing, thereby determining the intensity of T (Wu et al., 2020). However, to reduce water loss, plants regulate T by closing stomata, particularly under high VPD conditions (Pieruschka et al., 2010). Studies have shown that there is no linear relationship between LAI and T (Gao et al., 2022); although high LAI means more leaves participate in T, leaf overlap may reduce the photosynthetic and T capacity of lower-layer leaves. Precipitation shows a significant negative correlation with T, as increased precipitation reduces VPD, decreasing the driving force for water vapor diffusion from leaves to the atmosphere, thereby lowering the rate of T. Moreover, precipitation is often accompanied by low light and cloud cover, reducing both photosynthesis and T demand. Additionally, after precipitation, plant roots may temporarily close stomata due to oxygen shortage to protect themselves (Sauter, 2013).

https://doi.org/10.5194/egusphere-2025-4325
Preprint. Discussion started: 21 October 2025

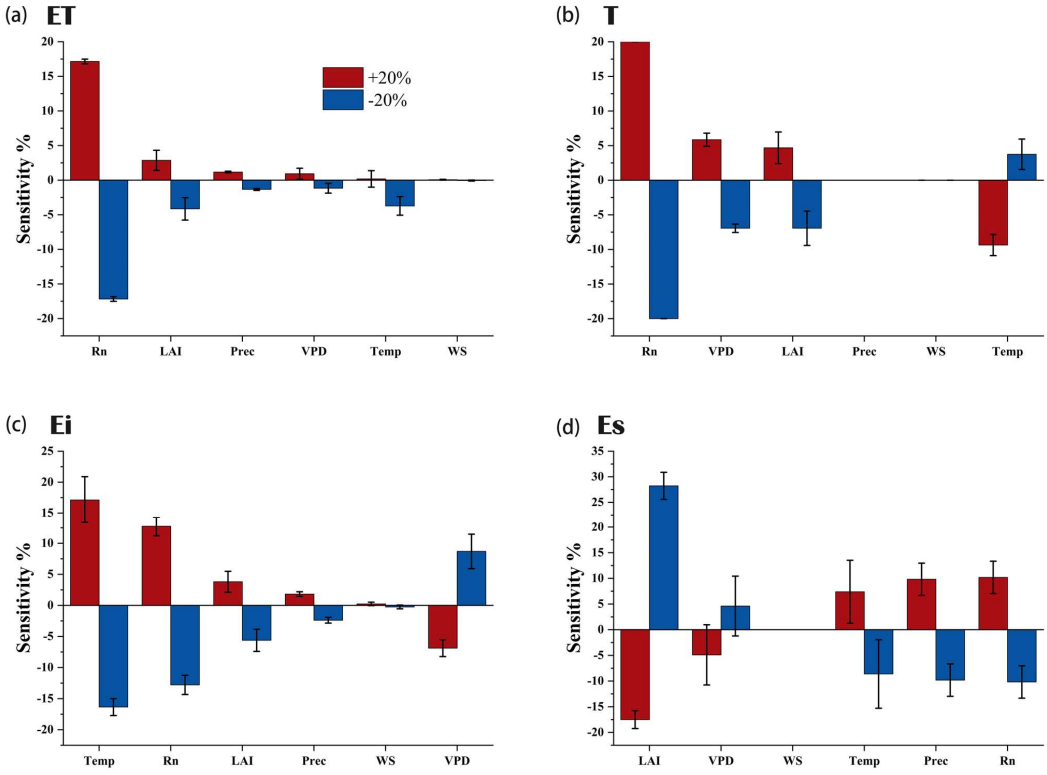

Fig. 10 Simulation results of ET and its components after a 20% increase (decrease) in a single input variable. Sensitivity is defined as (changed the input − unchanged)/unchanged, and black vertical lines mark the standard deviation of multiple models.

The seasonality of ET components simulated by the model at these sites seems to be explained by ecological mechanisms, but the model needs to be analyzed in more detail. We performed sensitivity analyses for the input variables of the three models, increasing (decreasing) a variable by 20% each time to observe its effect on the simulation results of ET and its components. As shown in Figure 10 a, consistent with the results studied by previous analysis, the primary sensitive input for ET is Rn, followed by LAI. In contrast to the linear regression results, all models demonstrated (with a small standard deviation) that the sensitive input for T is Rn, followed by VPD. In addition, a positive perturbation (negative perturbation) is applied to the temperature, but the result is the opposite for T.

https://doi.org/10.5194/egusphere-2025-4325
Preprint. Discussion started: 21 October 2025

Too sensitive to temperature and radiation in Ei simulations, which may be very different from the actual situation. After changing the temperature by 20%, the total amount of EI changes by more than 15%. Temperature and radiation are involved in canopy interception because evaporation rates are calculated, which is an important part of simulating Ei dynamics, but should be limited. In fact, the total amount of canopy interception evaporation will only be affected by two factors, the amount of precipitation and the density of canopy leaves, and other environmental factors just affect the evaporation rate.

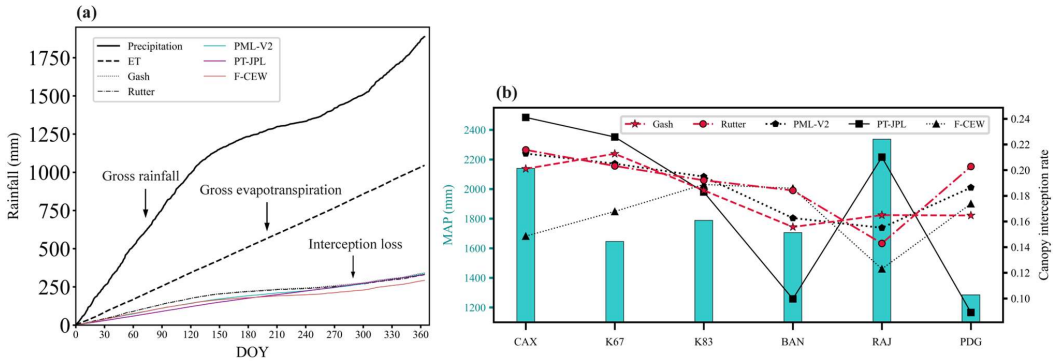

Fig. 11. (a) shows the multi-year averaged value of cumulative precipitation, evapotranspiration, and simulated canopy interception. **(b)** depicts canopy interception rates (interception/precipitation) simulated by different models across various sites, with different line types representing different models; the cyan bar graph indicates mean annual precipitation (MAP) for each site.

Combining two independent Ei models (See supplementary materials for details), we calculated the canopy interception evaporation data for these stations, and we divided the annual total canopy interception evaporation by the total annual precipitation at each station to obtain the canopy interception rate (Figure 11). We used the average of the Gash and Rutter models as the average Ei to evaluate the simulation of the other three ET models for this part. We found that the average canopy interception rate in the Amazon forest was 18% (±2.4), with Ei accounting for 31% (±4.2) of total ET. Overall, Forest-CEW underestimated the mean Ei by 12.4%, while the simulation results of the remaining models showed little difference. Site-specific analysis indicated that Forest-CEW underestimated Ei at the tropical rainforest sites CAX and K67; PT-JPL severely underestimated Ei at the BAN and PDG sites while

https://doi.org/10.5194/egusphere-2025-4325
Preprint. Discussion started: 21 October 2025

overestimating it in the seasonal forest at RJA. Since the Ei calculation module in PML-V2 approximates the Gash model, its simulations at various sites closely matched the average levels of Rutter and Gash.

3.4 Model mechanisms and limitations

Different models have varying sensitivities to inputs (Talsma et al., 2018). We try to explain the reasons for this by analyzing the components of the model, and the Forest-CEW model relates canopy interception with LAI and precipitation through a simple linear relationship; The PML-v2 model distinguishes between the process of maximum water holding capacity on the leaf surface under rainfall events and the drying rate of the canopy during the rainfall interval; The PT-JPL model cleverly depicts canopy wetting through RH and canopy radiation. The difference between the Penman-Monteith and Priestley-Taylor models usually depends on the parameterization of the α in the Priestley-Taylor equation and the resistance factor in the Penman-Monteith equation (Talsma et al., 2018). But PT-JPL's use of RH instead of precipitation to describe canopy humidity may underestimate Ei after heavy rain, because RH is not that sensitive. Due the Forest-CEW did not design the Es module, Figure 10 d shows the results of the other two models. In line with the reality, the Es results of positive perturbation (negative perturbation) applied to LAI are reversed, because the denser the canopy leaves, the less precipitation can penetrate to the surface. Moreover, the large standard deviations of VPD and other environmental variables indicate that the designs of the two models are incorrect.

From a more detailed perspective, tropical rainforests possess a complex multi-layered canopy structure, and microclimatic conditions such as local wind speed, relative humidity, and solar radiation can influence the drying rate of the canopy. The age composition of canopy leaves can also have a significant impact, as older leaves with higher lignification contribute to more runoff (Chavana-Bryant et al., 2017). Studies have shown that trees exhibit more complex transpiration activities and that eddy flux towers are difficult to measure (Fisher et al., 2007). More importantly, in addition to the interception and evaporation of precipitation during the dry and wet seasons, leaf

https://doi.org/10.5194/egusphere-2025-4325
Preprint. Discussion started: 21 October 2025

surfaces can also experience water condensation due to fog or temperature differences between day and night. Frequent persistent dense fog is an important source of water input for vegetation (Liu et al., 2010). Dense fog not only causes water to adhere to vegetation but also directly supplies water to plant leaves (Eller et al., 2016). Furthermore, the water film generated by dense fog covers the leaf surface, inhibiting stomatal respiration on the leaves, which in turn affects the evapotranspiration of the forest canopy. In different forests, the frequency and duration of leaf wetness can vary greatly due to environmental and topographical differences. Although this process is rarely studied, it is important to note that it can serve as an explanation for the inadequacies of the model.

The impact of climate extremes on the model remains unclear. Climate systems exhibit complex variability, and when multi-year averages are taken, the impacts of short-term extreme climatic events or anomalous years may be smoothed out (Hegerl et al., 2006). Additionally, the water supply limitations for plant T still need consideration (Li et al., 2023). In arid or semi-arid regions and areas with deep-rooted vegetation, soil water or groundwater storage might contribute more to vegetation evaporation than precipitation. In these regions, during periods of insufficient dry season precipitation, vegetation relies on deep soil water or groundwater to supplement ET, and stem water storage can also alleviate drought stress. However, in other regions, plants may experience water stress due to prolonged drought, and the occurrence and coping mechanisms for such stress still require further research. It is noteworthy that an improved version of the ET model addressing soil water constraints has been actively promoted (Purdy et al., 2018), which will greatly assist in tackling climate change and hydrodynamics.

6. Conclusions

In this study, we simulated and analyzed ET and its components at 7 flux tower sites in Amazon. First of all, there is still a certain deviation between the simulated value of the ET model in the Amazon forest and the observed value, and the simulation ability of the dry season is much stronger than that of the wet season. The Forest-CEW R^2

https://doi.org/10.5194/egusphere-2025-4325
Preprint. Discussion started: 21 October 2025

was 0.64, the PT-JPL was 0.43, and the PML-V2 was only 0.29, but the average results of the three models captured the approximate seasonality. ET in the Amazon forest exhibits strong seasonal variation controlled by Rn, while seasonality in T is mainly controlled by VPD. Second, the models CV of EI and ES indicates that the model has serious problems with the allocation of these two parts, and the proportion of Ei is much larger than that of Es in complex tropical forests, and improving Ei will improve the ET model

The sensitivity analysis of the model to the input variables showed that Rn was the main driving variable of ET and T of the model, with a sensitivity of 20%, temperature was the main driver of Ei, accounting for 17%, and LAI was the main driver of Es, but it produced negative effects. Different ET models characterize Ei differently, but the sensitivity of this module to the input variables differs from real-world conditions. Future improvements to the ET model should take into account more refined canopy interception. This seasonal analysis of ET and its components provides a window into the mechanisms underlying vegetation in the Amazon, suggesting that seasonal responses to environmental drivers are complex and diverse.

Data availability

The LBA eddy covariance towers data can be requested on: http://dx.doi.org/10.3334/ORNLDAAC/1174 (Accessed January 20, 2025), the LAI data: https://ladsweb.modaps.eosdis.nasa.gov/missions-and-measurements/products/MOD15A2H#overview (Accessed January 20, 2025), and the NDVI data: https://daac.ornl.gov/cgi-bin/dsviewer.pl?ds_id=2187 (Accessed January 20, 2025). The true color RGB image comes from MODIS/Terra Surface Reflectance 8-Day L3 Global 500m SIN Grid V061, which can be requested on : https://www.earthdata.nasa.gov/data/catalog/lpcloud-mod09a1-061 (Accessed July 30, 2025).

CRediT authorship contribution statement

L.L. : Writing - original draft, Writing - review & editing, Conceptualization, Methodology, Validation, Formal

https://doi.org/10.5194/egusphere-2025-4325
Preprint. Discussion started: 21 October 2025

analysis, Visualization, Software. **J.L.** : Writing - review & editing. **Z.T.** : provides the main research ideas of the paper and the review of the paper. All authors have read and agreed to the published version of the manuscript.

Declaration of Competing Interest

The authors declare that they have no known competing financial interests or personal relationships that could have appeared to influence the work reported in this paper.

Acknowledgements

This study was supported by the Major Program for Basic Research Project of Yunnan Province (grant No. 202101BC070002); the National Natural Science Foundation of China (grant No. 41771099, 41861023); and the Yunnan Province Department of Science and Technology and Yunnan University "Double World Class" Joint Construction Fund Project in 2023 (202301BF070001-015).

References

Batalha, M. A.: Análise da Vegetação de ARIE Cerrado Pé-de-Gigante (Santa Rita do Passa Quatro, SP)., 1997.

Bonan, G. B.: Forests and Climate Change: Forcings, Feedbacks, and the Climate Benefits of Forests, Science, 320, 1444–1449, https://doi.org/10.1126/science.1155121, 2008.

Borma, L. S., da Rocha, H. R., Cabral, O. M., von Randow, C., Collicchio, E., Kurzatkowski, D., Brugger, P. J., Freitas, H., Tannus, R., Oliveira, L., Rennó, C. D., and Artaxo, P.: Atmosphere and hydrological controls of the evapotranspiration over a floodplain forest in the Bananal Island region, Amazonia, J. Geophys. Res. Biogeosciences, 114, https://doi.org/10.1029/2007JG000641, 2009.

Campbell, G. S. and Norman, J. M.: An Introduction to Environmental Biophysics, 1977.

Carswell, F. E., Costa, A. L., Palheta, M., Malhi, Y., Meir, P., Costa, J. de P. R., Ruivo, M. de L., Leal, L. do S. M., Costa, J. M. N., Clement, R. J., and Grace, J.: Seasonality in CO2 and H2O flux at an eastern Amazonian rain forest, J. Geophys. Res. Atmospheres, 107, LBA 43-1-LBA 43-16, https://doi.org/10.1029/2000JD000284, 2002.

Chavana-Bryant, C., Malhi, Y., Wu, J., Asner, G. P., Anastasiou, A., Enquist, B. J., Cosio Caravasi, E. G., Doughty, C. E., Saleska, S. R., Martin, R. E., and Gerard, F. F.: Leaf aging of Amazonian canopy trees as revealed

https://doi.org/10.5194/egusphere-2025-4325
Preprint. Discussion started: 21 October 2025

by spectral and physiochemical measurements., New Phytol., 214, 1049–1063, https://doi.org/10.1111/nph.13853, 2017.

Costa, M. H., Biajoli, M. C., Sanches, L., Malhado, A. C. M., Hutyra, L. R., da Rocha, H. R., Aguiar, R. G., and de Araújo, A. C.: Atmospheric versus vegetation controls of Amazonian tropical rain forest evapotranspiration: Are the wet and seasonally dry rain forests any different?, J. Geophys. Res. Biogeosciences, 115, https://doi.org/10.1029/2009JG001179, 2010.

Duarte, M. M., Moral, R. de A., Guillemot, J., Zuim, C. I. F., Potvin, C., Bonat, W. H., Stape, J. L., and Brancalion, P. H. S.: High tree diversity enhances light interception in tropical forests, J. Ecol., 109, 2597–2611, https://doi.org/10.1111/1365-2745.13669, 2021.

Eller, C. B., Lima, A. L., and Oliveira, R. S.: Cloud forest trees with higher foliar water uptake capacity and anisohydric behavior are more vulnerable to drought and climate change, New Phytol., 211, 489–501, https://doi.org/10.1111/nph.13952, 2016.

Fisher, J. B., Baldocchi, D. D., Misson, L., Dawson, T. E., and Goldstein, A. H.: What the towers don't see at night: nocturnal sap flow in trees and shrubs at two AmeriFlux sites in California., Tree Physiol., 27, 597–610, https://doi.org/10.1093/treephys/27.4.597, 2007.

Fisher, J. B., Tu, K. P., and Baldocchi, D. D.: Global estimates of the land–atmosphere water flux based on monthly AVHRR and ISLSCP-II data, validated at 16 FLUXNET sites, Remote Sens. Environ., 112, 901–919, https://doi.org/10.1016/j.rse.2007.06.025, 2008.

Fisher, J. B., Malhi, Y., Bonal, D., Da Rocha, H. R., De Araújo, A. C., Gamo, M., Goulden, M. L., Hirano, T., Huete, A. R., Kondo, H., Kumagai, T., Loescher, H. W., Miller, S., Nobre, A. D., Nouvellon, Y., Oberbauer, S. F., Panuthai, S., Roupsard, O., Saleska, S., Tanaka, K., Tanaka, N., Tu, K. P., and Von Randow, C.: The land–atmosphere water flux in the tropics, Glob. Change Biol., 15, 2694–2714, https://doi.org/10.1111/j.1365-2486.2008.01813.x, 2009.

Fisher, J. B., Melton, F., Middleton, E., Hain, C., Anderson, M., Allen, R., McCabe, M. F., Hook, S., Baldocchi, D., Townsend, P. A., Kilic, A., Tu, K., Miralles, D. D., Perret, J., Lagouarde, J.-P., Waliser, D., Purdy, A. J., French, A., Schimel, D., Famiglietti, J. S., Stephens, G., and Wood, E. F.: The future of evapotranspiration: Global requirements for ecosystem functioning, carbon and climate feedbacks, agricultural management, and water resources, Water Resour. Res., 53, 2618–2626, https://doi.org/10.1002/2016WR020175, 2017.

Fleischmann, A. S., Laipelt, L., Papa, F., Paiva, R. C. D. de, de Andrade, B. C., Collischonn, W., Biudes, M. S., Kayser, R., Prigent, C., Cosio, E., Machado, N. G., and Ruhoff, A.: Patterns and drivers of evapotranspiration in South American wetlands, Nat. Commun., 14, 6656, https://doi.org/10.1038/s41467-023-42467-0, 2023.

Gan, G. and Liu, Y.: Inferring transpiration from evapotranspiration: A transpiration indicator using the Priestley-Taylor coefficient of wet environment, Ecol. Indic., 110, 105853, https://doi.org/10.1016/j.ecolind.2019.105853, 2020.

Gao, G., Wang, D., Zha, T., Wang, L., and Fu, B.: A global synthesis of transpiration rate and evapotranspiration partitioning in the shrub ecosystems, J. Hydrol., 606, 127417,

https://doi.org/10.5194/egusphere-2025-4325
Preprint. Discussion started: 21 October 2025

https://doi.org/10.1016/j.jhydrol.2021.127417, 2022.

Gao, X., Huete, A. R., Ni, W., and Miura, T.: Optical–Biophysical Relationships of Vegetation Spectra without Background Contamination, Remote Sens. Environ., 74, 609–620, https://doi.org/10.1016/S0034-4257(00)00150-4, 2000.

Gomis-Cebolla, J., Jimenez, J. C., Sobrino, J. A., Corbari, C., and Mancini, M.: Intercomparison of remote-sensing based evapotranspiration algorithms over amazonian forests, Int. J. Appl. Earth Obs. Geoinformation, 80, 280–294, https://doi.org/10.1016/j.jag.2019.04.009, 2019.

Grossiord, C., Buckley, T. N., Cernusak, L. A., Novick, K. A., Poulter, B., Siegwolf, R. T. W., Sperry, J. S., and McDowell, N. G.: Plant responses to rising vapor pressure deficit, New Phytol., 226, 1550–1566, https://doi.org/10.1111/nph.16485, 2020.

Gu, C., Ma, J., Zhu, G., Yang, H., Zhang, K., Wang, Y., and Gu, C.: Partitioning evapotranspiration using an optimized satellite-based ET model across biomes, Agric. For. Meteorol., 259, 355–363, https://doi.org/10.1016/j.agrformet.2018.05.023, 2018.

Hegerl, G. C., Karl, T. R., Allen, M., Bindoff, N. L., Gillett, N., Karoly, D., Zhang, X., and Zwiers, F.: Climate Change Detection and Attribution: Beyond Mean Temperature Signals, J. Clim., 19, 5058–5077, https://doi.org/10.1175/JCLI3900.1, 2006.

Kalácska, M., Calvo-Alvarado, J. C., and Sánchez-Azofeifa, G. A.: Calibration and assessment of seasonal changes in leaf area index of a tropical dry forest in different stages of succession, Tree Physiol., 25, 733–744, https://doi.org/10.1093/treephys/25.6.733, 2005.

Kruijt, B., Elbers, J. A., von Randow, C., Araújo, A. C., Oliveira, P. J., Culf, A., Manzi, A. O., Nobre, A. D., Kabat, P., and Moors, E. J.: THE ROBUSTNESS OF EDDY CORRELATION FLUXES FOR AMAZON RAIN FOREST CONDITIONS, Ecol. Appl., 14, 101–113, https://doi.org/10.1890/02-6004, 2004.

Li, X., Yang, Y., Zhou, X., Han, S., Li, H., Yang, Y., and Hao, X.: Accuracy evaluation of ET and its components from three remote sensing ET models and one process based hydrological model using ground measured eddy covariance and sap flow, J. Hydrol., 626, 130374, https://doi.org/10.1016/j.jhydrol.2023.130374, 2023.

Liu, W., Liu, W., Li, P., Duan, W., and Li, H.: Dry season water uptake by two dominant canopy tree species in a tropical seasonal rainforest of Xishuangbanna, SW China, Agric. For. Meteorol., 150, 380–388, https://doi.org/10.1016/j.agrformet.2009.12.006, 2010.

Lopes, D. de C., Neto, A. J. S., Queiroz, M. G. de, Souza, L. S. B. de, Zolnier, S., and Silva, T. G. F. da: Sparse Gash model applied to seasonal dry tropical forest, J. Hydrol., 590, 125497, https://doi.org/10.1016/j.jhydrol.2020.125497, 2020.

Luo, L.-X., Sun, Z.-Y., and Tan, Z.-H.: Climate Seasonality of Tropical Evergreen Forest Region, Water, 16, https://doi.org/10.3390/w16050749, 2024.

Maes, W. H., Pagán, B. R., Martens, B., Gentine, P., Guanter, L., Steppe, K., Verhoest, N. E. C., Dorigo, W.,

https://doi.org/10.5194/egusphere-2025-4325
Preprint. Discussion started: 21 October 2025

Li, X., Xiao, J., and Miralles, D. G.: Sun-induced fluorescence closely linked to ecosystem transpiration as evidenced by satellite data and radiative transfer models, Remote Sens. Environ., 249, 112030, https://doi.org/10.1016/j.rse.2020.112030, 2020.

Matsuo, T., Martínez-Ramos, M., Bongers, F., van der Sande, M. T., and Poorter, L.: Forest structure drives changes in light heterogeneity during tropical secondary forest succession, J. Ecol., 109, 2871–2884, https://doi.org/10.1111/1365-2745.13680, 2021.

Melo, D. C. D., Anache, J. A. A., Borges, V. P., Miralles, D. G., Martens, B., Fisher, J. B., Nóbrega, R. L. B., Moreno, A., Cabral, O. M. R., Rodrigues, T. R., Bezerra, B., Silva, C. M. S., Neto, A. A. M., Moura, M. S. B., Marques, T. V., Campos, S., Nogueira, J. S., Rosolem, R., Souza, R. M. S., Antonino, A. C. D., Holl, D., Galleguillos, M., Perez-Quezada, J. F., Verhoef, A., Kutzbach, L., Lima, J. R. S., Souza, E. S., Gassman, M. I., Perez, C. F., Tonti, N., Posse, G., Rains, D., Oliveira, P. T. S., and Wendland, E.: Are Remote Sensing Evapotranspiration Models Reliable Across South American Ecoregions?, Water Resour. Res., 57, e2020WR028752, https://doi.org/10.1029/2020WR028752, 2021.

Miralles, D. G., Jiménez, C., Jung, M., Michel, D., Ershadi, A., McCabe, M. F., Hirschi, M., Martens, B., Dolman, A. J., Fisher, J. B., Mu, Q., Seneviratne, S. I., Wood, E. F., and Fernández-Prieto, D.: The WACMOS-ET project – Part 2: Evaluation of \hack\break global terrestrial evaporation data sets, Hydrol. Earth Syst. Sci., 20, 823–842, https://doi.org/10.5194/hess-20-823-2016, 2016.

Morillas, L., Leuning, R., Villagarcía, L., García, M., Serrano-Ortiz, P., and Domingo, F.: Improving evapotranspiration estimates in Mediterranean drylands: The role of soil evaporation, Water Resour. Res., 49, 6572–6586, https://doi.org/10.1002/wrcr.20468, 2013.

Novick, K. A., Ficklin, D. L., Stoy, P. C., Williams, C. A., Bohrer, G., Oishi, A. C., Papuga, S. A., Blanken, P. D., Noormets, A., Sulman, B. N., Scott, R. L., Wang, L., and Phillips, R. P.: The increasing importance of atmospheric demand for ecosystem water and carbon fluxes, Nat. Clim. Change, 6, 1023–1027, https://doi.org/10.1038/nclimate3114, 2016.

Penman, H. L. and Keen, B. A.: Natural evaporation from open water, bare soil and grass, Proc. R. Soc. Lond. Ser. Math. Phys. Sci., 193, 120–145, https://doi.org/10.1098/rspa.1948.0037, 1948.

Pieruschka, R., Huber, G., and Berry, J. A.: Control of transpiration by radiation, Proc. Natl. Acad. Sci., 107, 13372–13377, https://doi.org/10.1073/pnas.0913177107, 2010.

Pinzon, J. E., Pak, E. W., Tucker, C. J., Bhatt, U. S., Frost, G. V., and Macander, M. J.: Global Vegetation Greenness (NDVI) from AVHRR GIMMS-3G+, 1981-2022, , https://doi.org/10.3334/ORNLDAAC/2187, 2023.

Pollard, D. and Thompson, S. L.: Use of a land-surface-transfer scheme (LSX) in a global climate model: the response to doubling stomatal resistance, Glob. Planet. Change, 10, 129–161, https://doi.org/10.1016/0921-8181(94)00023-7, 1995.

Priestley, C. H. B. and Taylor, R. J.: On the Assessment of Surface Heat Flux and Evaporation Using Large-Scale Parameters, Mon. Weather Rev., 100, 81–92, https://doi.org/10.1175/1520-0493(1972)100<0081:OTAOSH>2.3.CO;2, 1972.

https://doi.org/10.5194/egusphere-2025-4325
Preprint. Discussion started: 21 October 2025

Purdy, A. J., Fisher, J. B., Goulden, M. L., Colliander, A., Halverson, G., Tu, K., and Famiglietti, J. S.: SMAP soil moisture improves global evapotranspiration, Remote Sens. Environ., 219, 1–14, https://doi.org/10.1016/j.rse.2018.09.023, 2018.

Restrepo-Coupe, N., Rocha, H. R. da, Hutyra, L. R., Araujo, A. C. da, Borma, L. S., Christoffersen, B., Cabral, O. M. R., Camargo, P. B. de, Cardoso, F. L., Costa, A. C. L. da, Fitzjarrald, D. R., Goulden, M. L., Kruijt, B., Maia, J. M. F., Malhi, Y. S., Manzi, A. O., Miller, S. D., Nobre, A. D., Randow, C. von, Sá, L. D. A., Sakai, R. K., Tota, J., Wofsy, S. C., Zanchi, F. B., and Saleska, S. R.: What drives the seasonality of photosynthesis across the Amazon basin? A cross-site analysis of eddy flux tower measurements from the Brasil flux network, Agric. For. Meteorol., 182–183, 128–144, https://doi.org/10.1016/j.agrformet.2013.04.031, 2013.

Restrepo-Coupe, N., Albert, L. P., Longo, M., Baker, I., Levine, N. M., Mercado, L. M., da Araujo, A. C., Christoffersen, B. O., Costa, M. H., Fitzjarrald, D. R., Galbraith, D., Imbuzeiro, H., Malhi, Y., von Randow, C., Zeng, X., Moorcroft, P., and Saleska, S. R.: Understanding water and energy fluxes in the Amazonia: Lessons from an observation-model intercomparison, Glob. Change Biol., 27, 1802–1819, https://doi.org/10.1111/gcb.15555, 2021.

Rocha, H., Freitas, H., Rosolem, R., Juárez, R., Tannus, R., Ligo, M., Cabral, O., and Dias, M.: Measurements of CO2 exchange over a woodland savanna (Cerrado Sensu stricto) in southeast Brasil, Biota Neotropica, 2, 1–11, https://doi.org/10.1590/S1676-06032002000100009, 2002.

da Rocha, H. R., Goulden, M. L., Miller, S. D., Menton, M. C., Pinto, L. D. V. O., de Freitas, H. C., and e Silva Figueira, A. M.: Seasonality of water and heat fluxes over a tropical forest in eastern amazonia, Ecol. Appl., 14, 22–32, https://doi.org/10.1890/02-6001, 2004.

da Rocha, H. R., Manzi, A. O., Cabral, O. M., Miller, S. D., Goulden, M. L., Saleska, S. R., R.-Coupe, N., Wofsy, S. C., Borma, L. S., Artaxo, P., Vourlitis, G., Nogueira, J. S., Cardoso, F. L., Nobre, A. D., Kruijt, B., Freitas, H. C., von Randow, C., Aguiar, R. G., and Maia, J. F.: Patterns of water and heat flux across a biome gradient from tropical forest to savanna in Brazil, J. Geophys. Res. Biogeosciences, 114, https://doi.org/10.1029/2007JG000640, 2009a.

da Rocha, H. R., Manzi, A. O., Cabral, O. M., Miller, S. D., Goulden, M. L., Saleska, S. R., R.-Coupe, N., Wofsy, S. C., Borma, L. S., Artaxo, P., Vourlitis, G., Nogueira, J. S., Cardoso, F. L., Nobre, A. D., Kruijt, B., Freitas, H. C., von Randow, C., Aguiar, R. G., and Maia, J. F.: Patterns of water and heat flux across a biome gradient from tropical forest to savanna in Brazil, J. Geophys. Res. Biogeosciences, 114, https://doi.org/10.1029/2007JG000640, 2009b.

Santos, S. N. M. and Costa, M. H.: A simple tropical ecosystem model of carbon, water and energy fluxes, Ecol. Model., 176, 291–312, https://doi.org/10.1016/j.ecolmodel.2003.10.032, 2004.

Sauter, M.: Root responses to flooding, Curr. Opin. Plant Biol., 16, 282–286, https://doi.org/10.1016/j.pbi.2013.03.013, 2013.

Schlesinger, W. H. and Jasechko, S.: Transpiration in the global water cycle, Agric. For. Meteorol., 189–190, 115–117, https://doi.org/10.1016/j.agrformet.2014.01.011, 2014.

https://doi.org/10.5194/egusphere-2025-4325
Preprint. Discussion started: 21 October 2025

Shuttleworth, W. J., Gash, J. H. C., Lloyd, C. R., Moore, C. J., Roberts, J., Filho, A. D. O. M., Fisch, G., De Paula Silva Filho, V., Ribeiro, M. D. N. G., Molion, L. C. B., De Abreu Sá, L. D., Nobre, J. C. A., Cabral, O. M. R., Patel, S. R., and Carvalho De Moraes, J.: Eddy correlation measurements of energy partition for Amazonian forest, Q. J. R. Meteorol. Soc., 110, 1143–1162, https://doi.org/10.1002/qj.49711046622, 1984.

Singh, B. and Szeicz, G.: The effect of intercepted rainfall on the water balance of a hardwood forest, Water Resour. Res., 15, 131–138, https://doi.org/10.1029/WR015i001p00131, 1979.

Talsma, C. J., Good, S. P., Miralles, D. G., Fisher, J. B., Martens, B., Jimenez, C., and Purdy, A. J.: Sensitivity of Evapotranspiration Components in Remote Sensing-Based Models, Remote Sens., 10, https://doi.org/10.3390/rs10101601, 2018.

Wei, Z., Yoshimura, K., Wang, L., Miralles, D. G., Jasechko, S., and Lee, X.: Revisiting the contribution of transpiration to global terrestrial evapotranspiration, Geophys. Res. Lett., 44, 2792–2801, https://doi.org/10.1002/2016GL072235, 2017.

Wu, J., Serbin, S. P., Ely, K. S., Wolfe, B. T., Dickman, L. T., Grossiord, C., Michaletz, S. T., Collins, A. D., Detto, M., McDowell, N. G., Wright, S. J., and Rogers, A.: The response of stomatal conductance to seasonal drought in tropical forests, Glob. Change Biol., 26, 823–839, https://doi.org/10.1111/gcb.14820, 2020.

Zhang, Y., Leuning, R., Hutley, L. B., Beringer, J., McHugh, I., and Walker, J. P.: Using long-term water balances to parameterize surface conductances and calculate evaporation at 0.05° spatial resolution, Water Resour. Res., 46, https://doi.org/10.1029/2009WR008716, 2010.

Zhang, Y., Kong, D., Gan, R., Chiew, F. H. S., McVicar, T. R., Zhang, Q., and Yang, Y.: Coupled estimation of 500 m and 8-day resolution global evapotranspiration and gross primary production in 2002–2017, Remote Sens. Environ., 222, 165–182, https://doi.org/10.1016/j.rse.2018.12.031, 2019.

Zhao, M., A, G., Liu, Y., and Konings, A. G.: Evapotranspiration frequently increases during droughts, Nat. Clim. Change, 12, 1024–1030, https://doi.org/10.1038/s41558-022-01505-3, 2022.